Estimation of resonant properties and amplification factors for Canadian Hydrographic Service tide gauge sites along the coast of British Columbia

Alexander B. Rabinovich, Denny C. Sinnott, Richard E. Thomson, and Fred E. Stephenson

Fisheries and Oceans Canada
Institute of Ocean Sciences
9860 West Saanich Road
Sidney, BC, V8L 4B2, Canada

2025

Canadian Technical Report of Hydrography and Ocean Sciences 391

Fisheries and Oceans Canada | Pêches et Océans Canada

Canada

Canadian Technical Report of Hydrography and Ocean Sciences

Technical reports contain scientific and technical information of a type that represents a contribution to existing knowledge, but which is not normally found in the primary literature. The subject matter is generally related to programs and interests of the Oceans and Science sectors of Fisheries and Oceans Canada.

Technical reports may be cited as full publications. The correct citation appears above the abstract of each report. Each report is abstracted in the data base Aquatic Sciences and Fisheries Abstracts.

Technical reports are produced regionally but are numbered nationally. Requests for individual reports will be filled by the issuing establishment listed on the front cover and title page.

Regional and headquarters establishments of Ocean Science and Surveys ceased publication of their various report series as of December 1981. A complete listing of these publications and the last number issued under each title are published in the Canadian Journal of Fisheries and Aquatic Sciences, Volume 38: Index to Publications 1981. The current series began with Report Number 1 in January 1982.

Rapport technique canadien sur l'hydrographie et les sciences océaniques

Les rapports techniques contiennent des renseignements scientifiques et techniques qui constituent une contribution aux connaissances actuelles mais que l'on ne trouve pas normalement dans les revues scientifiques. Le sujet est généralement rattaché aux programmes et intérêts des secteurs des Océans et des Sciences de Pêches et Océans Canada.

Les rapports techniques peuvent être cités comme des publications à part entière. Le titre exact figure au-dessus du résumé de chaque rapport. Les rapports techniques sont résumés dans la base de données Résumés des sciences aquatiques et halieutiques.

Les rapports techniques sont produits à l'échelon régional, mais numérotés à l'échelon national. Les demandes de rapports seront satisfaites par l'établissement auteur dont le nom figure sur la couverture et la page de titre.

Les établissements de l’ancien secteur des Sciences et Levés océaniques dans les régions et à l'administration centrale ont cessé de publier leurs diverses séries de rapports en décembre 1981. Vous trouverez dans l'index des publications du volume 38 du Journal canadien des sciences halieutiques et aquatiques, la liste de ces publications ainsi que le dernier numéro paru dans chaque catégorie. La nouvelle série a commencé avec la publication du rapport numéro 1 en janvier 1982.

Canadian Technical Report of
Hydrography and Ocean Sciences 391

2025

ESTIMATION OF RESONANT PROPERTIES AND AMPLIFICATION FACTORS FOR CANADIAN HYDROGRAPHIC SERVICE TIDE GAUGE SITES ALONG THE COAST OF BRITISH COLUMBIA

by

Alexander B. Rabinovich, Denny C. Sinnott, Richard E. Thomson, and Fred E. Stephenson

Fisheries and Oceans Canada
Institute of Ocean Sciences
9860 West Saanich Road
Sidney, BC, V8L 4B2, Canada

Cat. No. Fs97-18/391E-PDF ISBN 978-0-660-76288-3 ISSN 1488-5417

Correct citation for this publication:

Rabinovich, A.B., Sinnott, D.C., Thomson, R.E., and Stephenson, F.E. 2025. Estimation of resonant properties and amplification factors for Canadian Hydrographic Service tide gauge sites along the coast of British Columbia. Can. Tech. Rep. Hydrogr. Ocean Sci. 391: v + 33 p.

CONTENTS

ABSTRACT

Rabinovich, A.B., Sinnott, D.C., Thomson, R.E., and Stephenson, F.E. 2025. Estimation of resonant properties and amplification factors for Canadian Hydrographic Service tide gauge sites along the coast of British Columbia. Can. Tech. Rep. Hydrogr. Ocean Sci. 391: v + 33 p.

The amplitude and periodicity of sea level oscillations in a basin are determined by its geometry and physical features. Each closed or semi-closed basin has a set of natural (eigen) modes that can be generated by external forcing and incoming open-ocean waves. The complicated coastline of British Columbia has a diversity of topographic features, including islands, straits, bays, fjords and waterways. These features can strongly amplify incoming tsunami waves, as occurred in Port Alberni, located at the head of the long and narrow Alberni Inlet, during the 1964 Alaska tsunami.

We have evaluated the amplification factor $H_j(\omega)$ for 16 selected Canadian Hydrographic Service (CHS) tide gauge sites (j = 1,…, 16) as a function of frequency (ω). The maximum value $H_j(\omega)$ = **23.2** and resonant period T_r = 102.4±5.2 h is for Port Alberni, exactly where the catastrophic 1964 tsunami event occurred. Significant $H_j(\omega)$ values were also found for Ucluelet (**14.5** at T_r = 23 min) and Pruth Bay (**12.7** at T_r = 24.4 min). All three sites may be characterized as "hot spots", i.e., as sites having an extreme response to the external forcing from incoming open-ocean waves. At Tofino, where more tsunamis have been recorded than at any other Canadian station (the "beacon station" for the Canadian Tsunami Warning Service), the amplification function has six comparable peaks, with $H_j(\omega)$ = **4.0 – 6.0** for resonant periods, T_r, from 5.4 to 57 min. This broadband response appears to be the reason why this station gives rise to amplified waves for a wide variety of incoming tsunamis.

RÉSUMÉ

Rabinovich, A.B., Sinnott, D.C., Thomson, R.E., and Stephenson, F.E. 2025. Estimation of resonant properties and amplification factors for Canadian Hydrographic Service tide gauge sites along the coast of British Columbia. Can. Tech. Rep. Hydrogr. Ocean Sci. 391: v + 33 p.

L'amplitude et la périodicité des oscillations du niveau de la mer dans un bassin sont déterminées par sa géométrie et ses caractéristiques physiques. Chaque bassin fermé ou semi-fermé possède un ensemble de modes naturels (propres) qui peuvent être générés par des forces externes et des vagues entrantes en pleine mer. Le littoral complexe de la Colombie-Britannique présente une diversité de caractéristiques topographiques, notamment des îles, des détroits, des baies, des fjords et des voies navigables. Ces caractéristiques peuvent amplifier considérablement les vagues de tsunami entrantes, comme cela s'est produit à Port Alberni, situé à la tête de la longue et étroite baie d'Alberni, lors du tsunami de 1964 en Alaska.

Nous avons évalué le facteur d'amplification $Hj(\omega)$ pour 16 sites de marégraphes du Service hydrographique du Canada (SHC) sélectionnés (j = 1, …, 16) en fonction de la fréquence (ω). La valeur maximale $Hj(\omega) = 23,2$ et la période de résonance $Tr = 102,4 \pm 5,2$ h concernent Port Alberni, exactement là où s'est produit le tsunami catastrophique de 1964. Des valeurs Hj(ω) significatives ont également été trouvées pour Ucluelet (14,5 à $Tr = 23$ min) et Pruth Bay (12,7 à $Tr = 24,4$ min). Ces trois sites peuvent être caractérisés comme des « points chauds », c'est-à-dire comme des sites présentant une réponse extrême à la force externe des vagues entrantes en pleine mer. À Tofino, où plus de tsunamis ont été enregistrés qu'à toute autre station canadienne (la « station phare » du Service canadien d'alerte aux tsunamis), la fonction d'amplification présente six pics comparables, avec $Hj(\omega) = 4,0 – 6,0$ pour les périodes de résonance, Tr, de 5,4 à 57 min. Cette réponse à large bande semble être la raison pour laquelle cette station génère des ondes amplifiées pour une grande variété de tsunamis entrants.

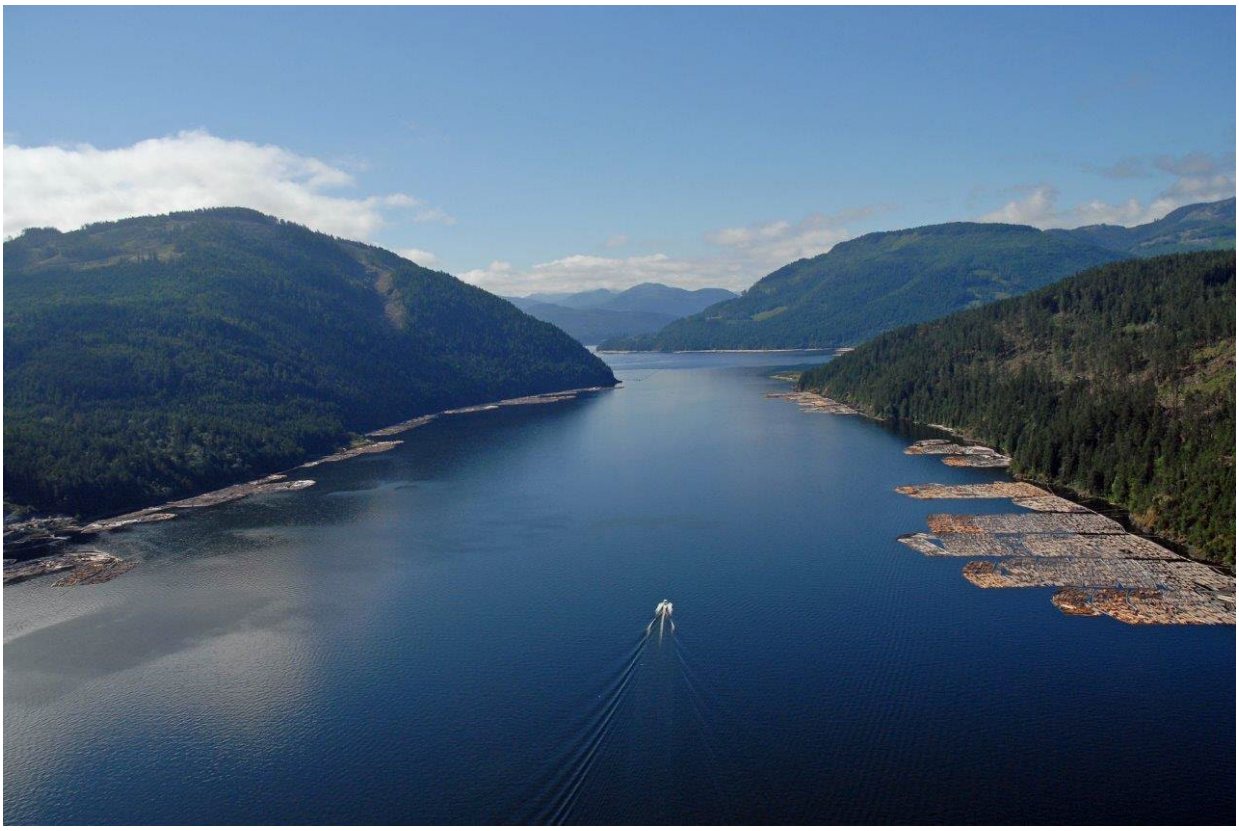

1. INTRODUCTION

Long ocean waves such as tsunamis arriving from the open ocean are strongly modified by regional and local topography and bathymetry. Continental shelves and adjacent bays, inlets and harbours can strongly transform and amplify incoming waves. These waves are significantly amplified near the coast due to local resonant effects. At specific sites, local harbour resonance plays a major role in amplification of long oceanic waves. In particular, although it has become obvious that meteorological tsunamis are observed all over the world [*Rabinovich,* 2020; *Vilibić et al.*, 2021] there are specific sites, called "*hot-spots*" (e.g., Ciutadella Inlet in the Balearic Islands, Spain; Vela Luka Bay, the Adriatic Sea, Croatia; and Nagasaki Bay in Japan), where such atmospherically-generated tsunamis occur regularly and have much larger heights than at more "ordinary" sites [*Monserrat et al.*, 2006; *Rabinovich,* 2020]. It is safe to assume that these extreme oscillation properties are determined by the specific geometry and physical properties of the corresponding basins (bays, inlets or harbours), in particular, by the high quality (Q) factors of these basins. The Q-factor is a measure of the energy damping in the system and, at the same time, characterizes the resonant amplification within the basin of arriving open-ocean waves: the higher the Q, the stronger

will be the amplification of the incoming waves and the slower the energy decay [*Miles*, 1974; *Rabinovich*, 2009].

Professor Omori (Japan) appears to have been the first to show that periods of tsunami waves are the same as those of regular background long waves for the same region [*Honda et al.*, 1908]. His explanation was that the bay or certain portion of the sea oscillates like a fluid pendulum with its own period. A number of papers related to the spectral analysis of tsunami records in various regions of the World Ocean have confirmed this conclusion and showed that the spectra of tsunamis from different earthquakes are usually similar at the same location but can be quite different for the same event for nearby locations [cf. *Loomis,* 1966; *Miller*, 1972; *Rabinovich*, 1997; *Zaytsev et al.,* 2016, 2017, 2021]. The same result for several tsunamis was also obtained for the coast of British Columbia [cf. *Rabinovich and Stephenson*, 2004; *Rabinovich et al.*, 2013, 2019].

British Columbia (BC) is characterized by a very long and complex coastline geometry. The distance from Juan de Fuca Strait in the south to Dixon Entrance at the north is about 900 km; the entire length of the coastline is approximately 27,300 km [*Thomson,* 1981]. The BC coastline encompasses a diversity of features, including islands, spits, straits, sounds, bays, inlets, fjords and other forms of waterways. All these features strongly affect incoming open-ocean tsunami waves. While some of these features, like the San Juan and Gulf islands, shelter the mainland or inner Vancouver Island coasts from devastating tsunami waves, the others can resonantly enhance these waves.

The major threat for the coast of British Columbia is from great trans-oceanic tsunamis generated by the strongest subduction earthquakes with source areas located along the Pacific Ring of Fire. Examples include the 1700 Cascadia (estimated momentum magnitude $M_w \sim 9.0$), the 1946 Aleutian (M_w 8.6), 1952 Kamchatka (M_w 9.0), 1957 Andreanof Islands (M_w 8.6). 1960 Chile (M_w 9.5), 1964 Alaska (M_w 9.2) and 2011 Tohoku (M_w 9.1) earthquakes. All of these events induced substantial seiche oscillations in bays, inlets, and harbours throughout the Pacific Ocean, including those in embayments along the BC coast [*Rabinovich et al.*, 2019]. The tsunami periods and wave heights recorded at various sites of the BC coast during these events were significantly different: at some sites tsunami waves were low amplitude, while at some others they were quite high, even catastrophic. It is evident that these differences are related to resonant (or counter-resonant) properties of the respective sites and also to specific filtering effects of certain straits and waterways. Therefore, estimation of eigen (resonant) periods and amplification factors for bays, inlets and harbours is a key

part of long-term tsunami forecasting [*Mofjeld et al.*, 1999, 2000]. The customary method of such estimations is numerical modelling [*Raichlen et al.*, 1983; *Mofjeld et al.,* 1999). Unfortunately, this method is very labor intensive and needs detailed bathymetry. For the BC coast, such high-resolution bathymetry is available only for a limited number of sites. However, some simple estimates of local topographic response can be obtained directly from sea level spectra without complicated numerical computations. This is the main purpose of the current study.

The most destructive tsunami event on the coast of British Columbia, and one of the most hazardous tsunami events in Canada, in general, occurred at Port Alberni after the 1964 Great Alaska (Good Friday) earthquake and, as indicated by *Murty* [1977, 1992], was caused by a strong resonance in Alberni Inlet. Detailed analysis of this event, provided by *Fine et al.* [2009], confirmed this speculation. The 1964 tsunami was the strongest seismic tsunami ever observed on the west coast of Canada, where it was recorded by practically all coastal tide gauges in operation at that time [*Rabinovich et al.*, 2019]. However, the main devastating effects and severe damage were reported only in two regions: at the towns of Alberni and Port Alberni[1] located at the head of Alberni Inlet, western coast of Vancouver Island (where 8-m waves were observed) [*Fine et al.*, 2009; *Rabinovich et al.,* 2019] and at Prince Rupert, northwestern British Columbia (2.7 m maximum wave height) [*Rabinovich et al.,* 2019; *Thomson et al.*, 2023]. This event clearly demonstrated the critical importance of local resonant effects on formation of destructive tsunamis along the coast. In the following section, the results of *Fine et al.* [2009] will be used to overview these effects for Alberni Inlet.

2. ALBERNI INLET RESONANCE

Alberni Inlet is a long (~40 km) and narrow (1-2 km) fjord (Figure 1) characterized by a deep (>250 m) southern part of the channel but rather shallow (~ 100 m) approaches in the relatively wide Barkley Sound located between the inlet and the continental shelf. On March 28, 1964, the towns of Alberni and Port Alberni, at the head of the inlet and about 65 km from the Pacific Ocean, were impacted by destructive tsunami waves generated by the 1964 Alaska earthquake. The waves caused wide-spread flooding and property damage estimated to be about 10 million (1964) dollars [*Murty,* 1977; *Clague et al.*, 2003].

[1] At present, these two cities are collectively known as Port Alberni.

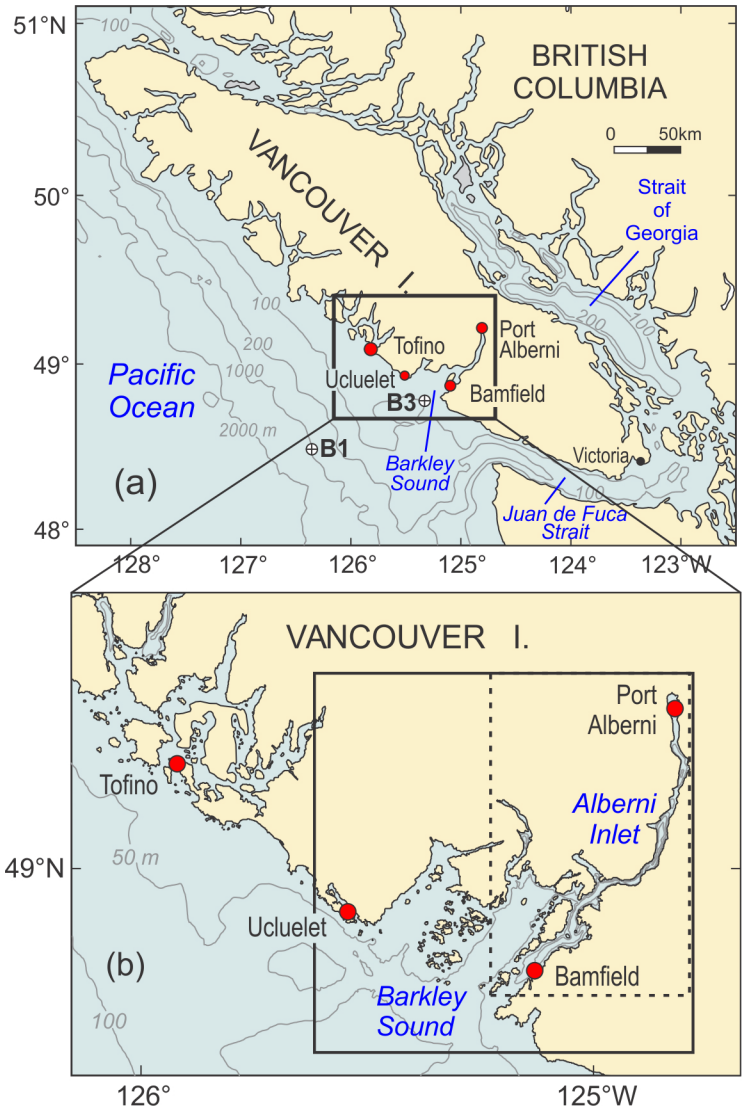

Figure 1. (a) Map of Vancouver Island (British Columbia) showing the locations of the CHS tide gauges (red circles). Labels B1 (1000 m depth) and B3 (85 m) indicate locations of reference computational points. (b) Map of Barkley Sound and Alberni Inlet showing domains of the two numerical models: model A (solid frame), which was used to examine characteristic wave properties of the Barkley Sound – Alberni Inlet system, and the innermost grid of model B (dashed frame), used for modeling tsunami waves (modified from *Fine et al.*, [2009]).

Tsunami wave heights in Port Alberni were estimated to exceed 8 m. The Port Alberni tide gauge was disabled temporarily and stopped working several times before the wave height maxima were reached (Fig.2a), but according to witness reports, the second wave was the highest in the series, reaching 6.4 m above tidal datum, as was determined from water marks on buildings and harbour

structures [*Wigen and White*, 1964]. The resulting flooding and property damage were made worse by the fact that the first two waves arrived around the time of the high (HW) tide (Fig. 2a).

A number of questions arose from this major event.

- *What is the physical mechanism responsible for the destructive tsunami oscillations observed in Port Alberni?*
- *Why did such strong oscillations occur specifically in this inlet?*
- *What kind of tsunami waves are likely to cause significant damage in this area in the future?*

It was assumed [cf. *Murty and Boilard*, 1970; *Murty*, 1992; *Clague et al*., 2003] that the 1964 event in Alberni Inlet had a resonant character with wave periods between 1.7 and 2 hours (Figure 2a). The averaged spectrum derived from the tide gauge oscillations (Figure 2b) shows a dominant peak with a period of approximately 1.8 hours (~110 min). The strong sea level response was due to the fact that the dominant period of the tsunami waves propagating from the source was near the fundamental period of the inlet [*Rabinovich et al.,* 2019]. The oscillations in the inlet were therefore resonantly generated by the arriving tsunami waves.

A number of studies [cf. *Murty and Boilard*, 1970; *Henry and Murty*, 1972; 1995] focused on explaining the observed 1964 tsunami oscillations in Alberni Inlet. However, the spatial resolution of these models and the accuracy of the bathymetry were insufficient for the region with such complicated topography. These models also did not resolve the detailed frequency spectrum and relative amplification of the long-wave oscillations in the inlet. Finally, the lack of reliable sea level observations is a key factor limiting our ability to estimate the spectral characteristics of the oscillations and to verify the numerical tsunami models in this area.

A new high-quality digital tide gauge installed at Port Alberni at the beginning of 2006 has provided a long time series of the background oscillations at the head of Alberni Inlet and has recorded several weak tsunamis [cf. *Stephenson and Rabinovich*, 2009]. These new precise instrumental data allowed us to examine the spectral properties of oscillations in the inlet and to verify the modelling results. Also, updated high-resolution bathymetric data enabled *Fine at al.* [2009] to construct an effective numerical model that enabled them to investigate the resonant characteristics of the Barkley Sound and Alberni Inlet system and to examine transformation and amplification of tsunami waves arriving from the open ocean.

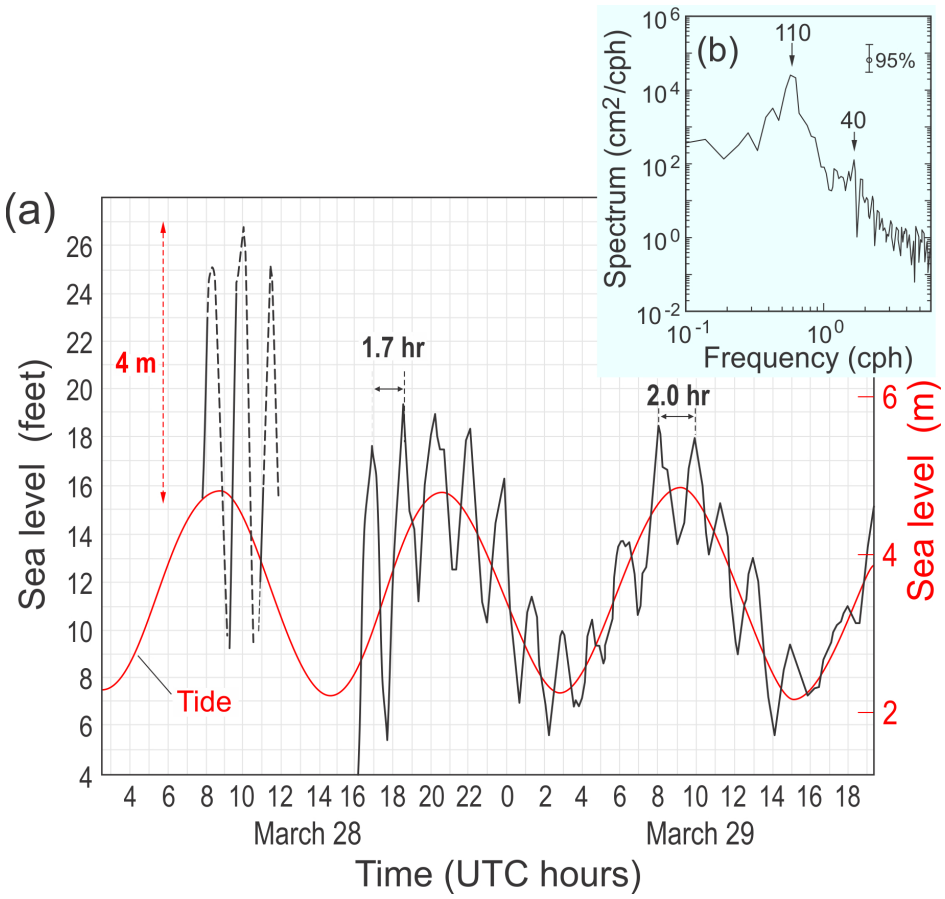

Figure 2. (a) A restored copy of Port Alberni tide gauge record of the Alaska tsunami of March 28, 1964 (from *Wigen and White* [1964]). The predicted tide is shown by the red line. The tide gauge stopped working at 04:00 PST on 28 March but resumed operation four hours later. The highest recorded sea level, about 4 m above high tide at 02:00 PST, was due to the second incoming tsunami wave, while the corresponding maximum (peak-to-through) wave height at Port Alberni was about 6 m, or larger, and occurred during the third, or later, wave. The exact number and maximum height of the largest tsunami wave are uncertain because of the 4-hour data gap. Oscillations at Alberni Inlet persisted for at least 48 hours, with wave periods from 1.7 to 2 hours. (b) Computed spectrum of the tsunami record in Port Alberni shown in (a) for the period between 08:00 PST on 28 March and 10:00 PST on 29 March. Periods (in min) of two main spectral peaks are indicated.

To examine longwave background oscillations in the Barkley Sound – Alberni Inlet system, *Fine at al.* [2009] used a linear shallow-water numerical model based on the finite-difference method; the model is similar to the well-known TUNAMI model [*Imamura*, 1996]. Random "red noise" fluctuations, reproducing the observed background noise, were used as an input on the outer side of the open boundary. A stationary autoregressive (AR) model of first order was used for this purpose;

the AR spectrum is a monotonic function decreasing according to a ω^{-2} power law, similar to the observed background spectra in the open ocean [*Kulikov et al.*, 1983; *Rabinovich*, 1997]. In contrast to a common method based on numerical simulation of monochromatic waves with select frequencies [cf. *Henry and Murty*, 1995], such a model is forced at its open boundary using waves with a continuous spectrum, which allows us to calculate the system response over a complete frequency range. The computational domain for the model is shown in Figure 1b. The model grid dimensions were 1213×1223 and the grid size was 50 m. The original version of this model was used previously to examine the resonant oscillations in the bays and inlets of Shikotan Island (Kuril Islands) [*Djumagaliev et al.*, 1994] and Menorca Island, the Balearic Islands [*Rabinovich et al.*, 1999].

Model sea-level time series were computed for Port Alberni and Bamfield. These time series were then used for spectral and cross-spectral analyses between the two sites. Similar analyses were also performed for two-month time series of the observed sea levels at these two sites. The remarkable agreement between the simulated and the observed spectra and cross-spectral characteristics (coherence, phase differences and admittance) for Bamfield and Port Alberni in the frequency range up to 2.5 cph suggests that this model is reliable and can provide realistic results, not just for these two stations, but for the entire computational area. (The plots for computed and observed coherences, phases and admittance functions are not shown here for brevity; see Figure 6 in *Fine et al.* [2009]).

The phase difference between the two sites is especially worth noting: it is step-like, with phase shifts near 0° or 180°. These shifts correspond exactly to the frequencies of the coherence minima. This is typical for a standing wave system; phase shifts and coherence minima are related to the nodal lines moving past Bamfield into the inlet with increasing frequency and indicating transition from one mode to the next one. The maximum amplitude response in Alberni Inlet (near 0.6 cph) corresponds to the fundamental (n = 0) mode, with the nodal line location further offshore from Bamfield, probably close to the entrance to Barkley Sound. For this mode, sea level oscillations at Bamfield and Port Alberni are in-phase (0°), but at Port Alberni (at the head of the inlet), this mode has much higher amplitude than at Bamfield, i.e., is close to the system entrance.

The observed background spectra, $S_b(\omega)$, were used to estimate the amplification functions of the corresponding sites, $H_j(\omega)$:

$$H_j(\omega) = \left[\frac{S_b(\omega)}{S_0(\omega)}\right]^{1/2}. \quad (1)$$

According to *Kulikov et al.* [1983] and *Rabinovich* [1997], the open ocean background spectrum in the tsunami frequency band can be presented as

$$S_0(\omega) = A\omega^{-2}, \tag{2}$$

where A is a near constant coefficient that is only slightly dependent on the region and weather conditions [cf. *Kovalev et al.*, 1991]. Based on Tofino and Bamfield measurements, *Fine et al.* [2009] estimated A = 0.125 cm^2/h. The results of their calculations of the observed amplification function at Port Alberni, $H_{\mathrm{PA}}(\omega)$, is shown in Figure 3. Earlier, the same approach (1) – (2) was used by *Rabinovich and Stephenson* [2004] to estimate $H_{\mathrm{j}}(\omega)$ for a number of the BC sites, but not for Port Alberni, where the digital tide gauge had not yet been installed.

The same coefficient was estimated by *Fine et al.* [2009] numerically. The resulting function presented in Figure 3 is in good agreement with the observations. There are three maxima of $H_{\mathrm{PA}}(\omega)$ with peak values at periods of approximately 102, 43 and 26 min. Estimation of eigen periods and the corresponding spatial modal structure (Figure 4) indicates that these periods are related to the fundamental (zeroth), first and second modes of the Barkley Sound - Alberni Inlet system shown in Figure 1.

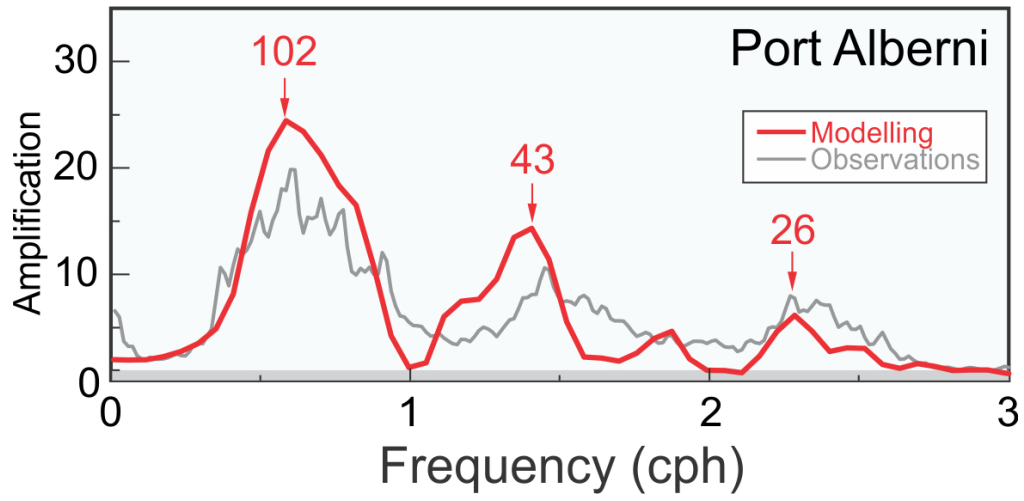

Figure 3. Observed and simulated amplification factors for Port Alberni. Periods (in min) of the main peaks are indicated. (Modified from *Fine et al.* [2009]).

The fundamental (zeroth) mode, known as the *Helmholtz mode*, is the most important. The maximum theoretical H_{PA} value at the main resonant period of 102 min[2] is about 25, the observed maximum is ~20. This means that a wave with this period, arriving from the open ocean, amplifies 20-25 times at the head of Alberni Inlet. Actually, the entire frequency band of high amplification, H_{PA} >15, is quite wide, ranging from 0.45 to 0.8 cph (periods of 135 to 75 min). According to these estimates, any low-frequency tsunami waves with dominant periods within this band would multiply more than 15 times at the head of Alberni Inlet, exactly in the area of the twin towns – Alberni and Port Alberni. This particular situation occurred during the 1964 Alaska tsunami, when tsunami waves incoming from the open ocean to the entrance of Barkley Sound had predominant frequencies of 0.4–0.8 cph (periods of 2.5–1.2 h) [*Rabinovich et al.*, 2019]. This appears to be the main reason for the damaging effects that took place in these two towns during the 1964 event [*Wigen and White*, 1964; *Murty*, 1977].

The incoming waves with resonant periods of the first (43 min) and second (26 min) modes are also amplified, but the H_{PA} values for these periods are substantially smaller than for the zeroth mode. In general, both the theoretical computations and observations demonstrate that Alberni Inlet plays the role of a low-frequency filter, transferring and amplifying long-period motions and strongly suppressing short-period waves. That is why moderate tsunamigenic earthquakes, even those located close by, are not dangerous for this region; such earthquakes have relatively small source areas and, consequently, produce higher-frequency tsunami waves that do not penetrate into the inlet. In contrast, major trans-oceanic earthquakes, such as the 1964 Alaska and 1960 Chile, have very large source regions and are responsible for extra-low frequency tsunami waves with dominant periods as long as 1-3 hours [cf. *Rabinovich et al.*, 2019]. Tsunami waves associated with these earthquakes present a high risk to Port Alberni and other sites located within Alberni Inlet.

Figure 4, constructed by *Fine et al.* [2009], provides additional insight into the spatial structure of the three main inlet modes and shows the relative sea level changes along a transect from the Barkley Sound entrance to Port Alberni (Figure 4a). This area can be divided into three parts: Barkley Sound, lower Alberni Inlet (up to the Sproat Narrows) and upper Alberni Inlet. For low frequencies (< 0.9 cph), the fundamental mode (n = 0) with a peak period of about 112 min strongly prevails in

[2] In fact, this mode has a relatively broad spectral peak with periods between 64 and 170 min (frequency range of 0.35-0.94 cph), which appears to be mostly due to the influence of Barkley Sound (Figure 1) and various angles of the incoming open-ocean waves [*Fine et al.*, 2009].

all three parts of the system (Figure 4c). This numerically estimated period almost precisely coincides with the period of maximum tsunami waves recorded at Port Alberni during the 1964 Alaska tsunami (Figure 1). When the frequency increases beyond 0.9 cph, the oscillation amplitudes decrease along the entire transect. For frequencies higher than 1.5 cph (for periods <40 min), Alberni Inlet and Barkley Sound oscillations become decoupled, as the upper Alberni Inlet is almost ‘‘blocked’’ by Sproat Narrows. The lower part of the inlet and Barkley Sound show minor amplification at these high frequencies.

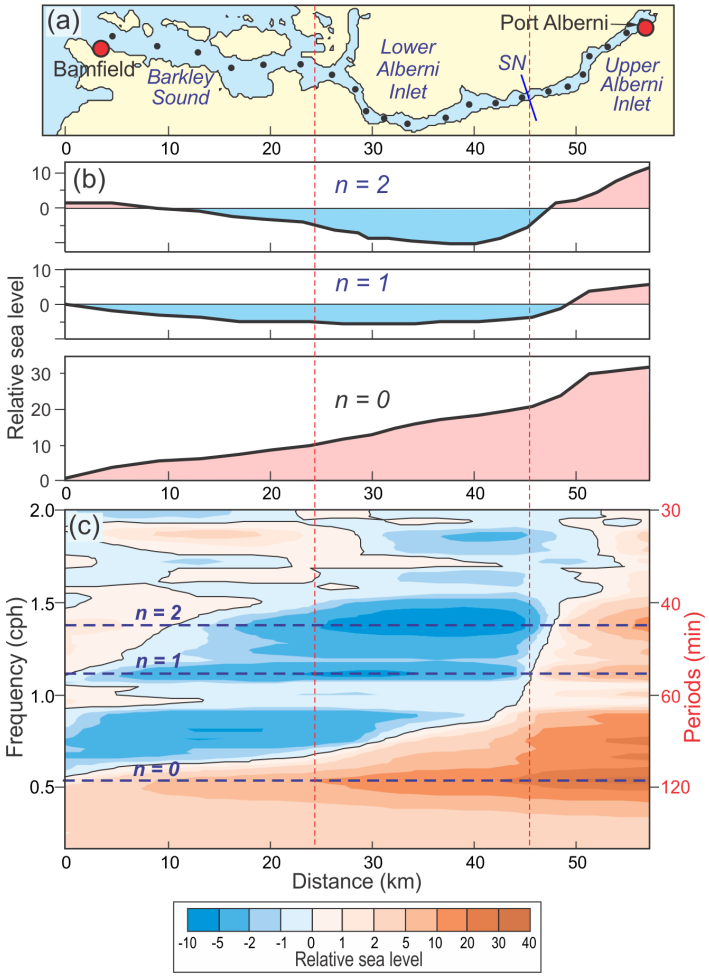

Figure 4. Along-channel computed structure of sea level oscillations in Barkley Sound and Alberni Inlet. (a) The computational domain of Barkley Sound and Alberni and along-channel transect with computational sites are denoted by the black dots; CHS tide gauges in Bamfield and Port Alberni are indicated by red circles. The vertical dashed (red) lines separate the three regions: Barkley Sound, lower Alberni Inlet and upper Alberni Inlet; label “SN” indicates Sproat Narrows. (b) Computed forms of three first modes (n = 0, 1 and 2). (c) Relative sea-level along-channel heights as function of frequency with frequencies of the first three modes indicated by horizontal dashed lines. (From *Fine et al.* [2009]).

The zeroth (Helmholtz) mode requires major attention. Theoretically, it has a single nodal line located in the open ocean close to the mouth of Barkley Sound and a single antinode on the opposite shore, i.e., at the head of the bay/inlet. The wavelength of this mode is equal to four times the length of the bay; a basin oscillating in this manner is known as a "*quarter-wave oscillator*" [*Mei,* 1992]. The Helmholtz mode is also known as the "*pumping mode*" (because it is related to periodic mass transport — pumping — through the open mouth [*Lee*, 1971]). This is exactly what we see for the Barkley Sound -Alberni Inlet system (Figure 4b, bottom plot). The along-channel transect of this mode indicates that the wave amplitude increases almost linearly from the nodal line, located oceanward from Bamfield, to Sproat Narrows and then, after an abrupt jump, gradually enhances to the very end of the inlet, the location of Port Alberni. Thus, the theoretical modelling results of *Fine et al.* [2009] perfectly explains the reason for the major tsunami event of 28 March 1964 at Alberni and Port Alberni (Figure 1).

In general, analysis of the 1964 tsunami tide gauge record from Port Alberni, combined with the numerical modelling results of *Fine et al.* [2009] seiche oscillations within the system Barkley Sound – Alberni Inlet, clearly demonstrate the crucial influence of resonant properties of local topography on the character and relative amplification of tsunami waves for the coast of British Columbia.

3. THEORETICAL BACKGROUND AND OPEN-OCEAN SPECTRUM

As was shown by *Rabinovich* [1997] and *Rabinovich and Stephenson* [2004], linear sea level oscillations $\zeta(t)$ recorded at time t by a tide gauge near the coast can be described as a convolution of the source $Z(t)$ and the topographic response function $w(t)$:

$$\zeta(t) = \int_0^\infty w(\tau)Z(t-\tau)d\tau. \quad (3)$$

In the spectral domain, (3) can be expressed in the form:

$$S(\omega) = W(\omega)E(\omega), \quad (4)$$

where ω is the angular frequency, $S(\omega)$ is the spectrum of sea levels, $W(\omega) = H^2(\omega)$ is the admittance function, $H(\omega)$ is the amplification function, describing the linear topographic transformation of long waves approaching the coast, and $E(\omega)$ is the open-ocean source spectrum. If we assume that the observed spectra can be presented in the form (4), the individual aspects of the observed spectrum

$S_j(\omega)$ at the *j*th site are related to the individual topographic function $H_j(\omega)$, while all general properties of this spectrum are associated with the source region (certainly, if the source is the same for different stations) (see *Rabinovich* [1997] for details). As was indicated above, ordinary background oscillations in the open ocean, $E(\omega) = S_0(\omega)$, can be presented in the form (2). Long-term bottom pressure measurements in the various regions of the Pacific Ocean [*Kulikov et al.*, 1983; *Rabinovich*, 1997] have demonstrated that, in the deep open ocean, function $S_0(\omega)$ is smooth and monotonic and almost universal. To check this and to estimate the optimum value of coefficient *A* in the open-ocean spectrum presented as $A\omega^{-2}$, we used the deep-ocean DART and ONC[3] stations. The location of these stations is shown in Figure 5.

For our spectral analysis, we selected two DART records (DARTs 46416 and 46419) for the period of 9 – 23 August 2021 and ONC records for the period of 10 – 20 October 2016. The DART data, with sampling interval Δt = 15-s, were downloaded following the instrument retrievals from the seafloor [cf. *Mungov et al.*, 2013; *Rabinovich and Eblé*, 2015]; the DART depths were 3450 m (46416) and 2804 m (46419). The ONC instruments are located in water depths from 96 m to 2654 m (Figure 5); for spectral analysis we used the averaged and cleaned data with sampling interval, Δt = 1 min [cf. *Rabinovich et al.*, 2023a]. To improve the spectral estimates, we applied a Kaiser-Bessel (KB) spectral window with half-window overlaps prior to the Fourier transform. The window length was chosen to be 1024 min, i.e., N = 4096 for DARTs (15-s data), yielding ν = 70 degrees of freedom, and N = 1024 for ONC (1-min data), ν = 52; the spectral resolution was Δf = 0.0586 cycles per hour (cph). The DART records had been de-tided by the NOAA National Centers for Environmental Information (NCEI); the ONC records were de-tided by the least squares method of tidal harmonic analysis [cf. *Pugh and Woodworth*, 2014; *Thomson and Emery*, 2024].

[3] DART = Deep-ocean Assessment and Reporting of Tsunamis, is an effective network of deep-ocean stations designed for continuous monitoring of tsunami waves in the open ocean and for early tsunami warning [cf. *Rabinovich and Eblé*, 2015]. ONC = Ocean Networks Canada is a network of ocean-bottom cable observatories hosted and operated by the University of Victoria. ONC stations are actively used to record and examine tsunami waves [cf. *Thomson et al.*, 2011; *Rabinovich et al.*, 2013, 2023; *Fine et al.*, 2015]

Figure 5. Map of coastal British Columbia showing the location of CHS coastal tide gauges (CHS S is the southern group, CHS N is the northern group), the ONC cabled ocean observatory network, and two DART buoys (46416 and 46419). ONC abbreviations: End = Endeavour, ODP = Ocean Drilling Program, BC = Barkley Canyon, CS = Clayquot Slope, FP = Folger Passage. TG abbreviations: PR = Port Renfrew, QCC = Queen Charlotte City (at present Daajing Giids).

To estimate the properties of the open-ocean tsunami spectra, we used these two DARTs, 46416 and 46419, and the deepest ONC station, ODP. Spectra from time series analysis are shown in Figure 6. It is important to emphasize that these three stations are located several hundred kilometers from each other, have different depths (3450 m, 2804 m and 2640 m, respectively) and different time periods (August 2021 for the DARTs and October 2016 for ODP). Moreover, the weather during the DART measurements was calm, while that during the ODP record coincided with an extremely strong storm [*Rabinovich et al.*, 2023a]. Nevertheless, the background spectra in the tsunami frequency band of 0.3 – 8 cph (periods of 3.3 hr – 7.5 min) were amazingly smooth, monotonic, consistent and well approximated by the ω^{-2} power law (Figure 6), in good agreement with the results of previous studies

of open-ocean sea level spectra [cf. *Kulikov et al.*, 1983; *Rabinovich*, 1997]. The coefficient A in expression (2) is found to be $A = 6.3\times10^{-3}$ cm^2·cph. The increase in the ODP spectrum at high frequencies (shaded area in Figure 6) is due to storm-generated IG-waves [cf. *Rabinovich and Eblé*, 2015].

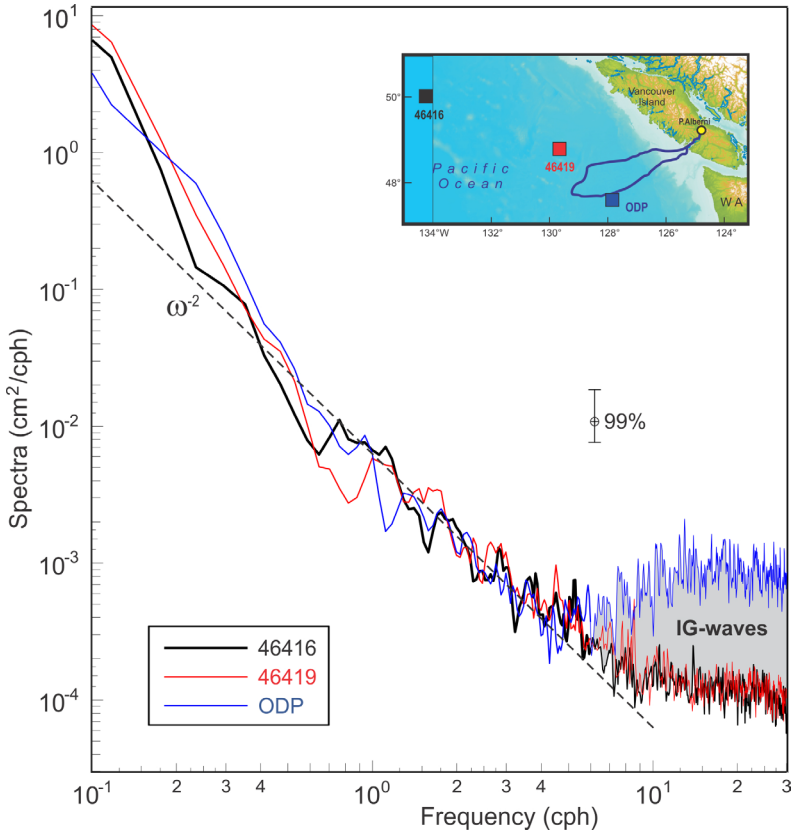

Figure 6. Open-ocean bottom pressure background spectra offshore from Vancouver Island for DARTs 46416 and 46419 (period of 9 – 22 August 2021) and ONC ODP (10 – 20 October 2016). The locations of the stations are shown in the inset. The dashed line indicates the ω^{-2} theoretical power law. The shaded area denotes the spectrum of storm-generated infragravity (IG) waves recorded at site ODP.

The spectral distributions of the open-ocean bottom pressure measurements shown in Figure 6, as well as similar results for many other deep-ocean sites around the world [cf. *Zaytsev et al.*, 2016, 2017; *Rabinovich et al.*, 2017], clearly demonstrate the universal character of $S_0(\omega)$. This means that individual peaks and troughs in the observed coastal spectra $S(\omega)$ are related to topographic influence, i.e., the resonant effects of the continental slope, shelf and bays/harbours [*Rabinovich,* 1997]. To examine the spectral evolution of the background spectra with decreasing depth

approaching the coast, we used data from three ONC stations located at different depths and offshore distances - Clayquot Slope (depth of 1258 m), Barkley Canyon-380 (380 m) and Folger Passage (96 m) – and compared them with the spectrum of DART 46416 (3450 m) (see Figure 5 for station locations). The results are shown in Figure 7.

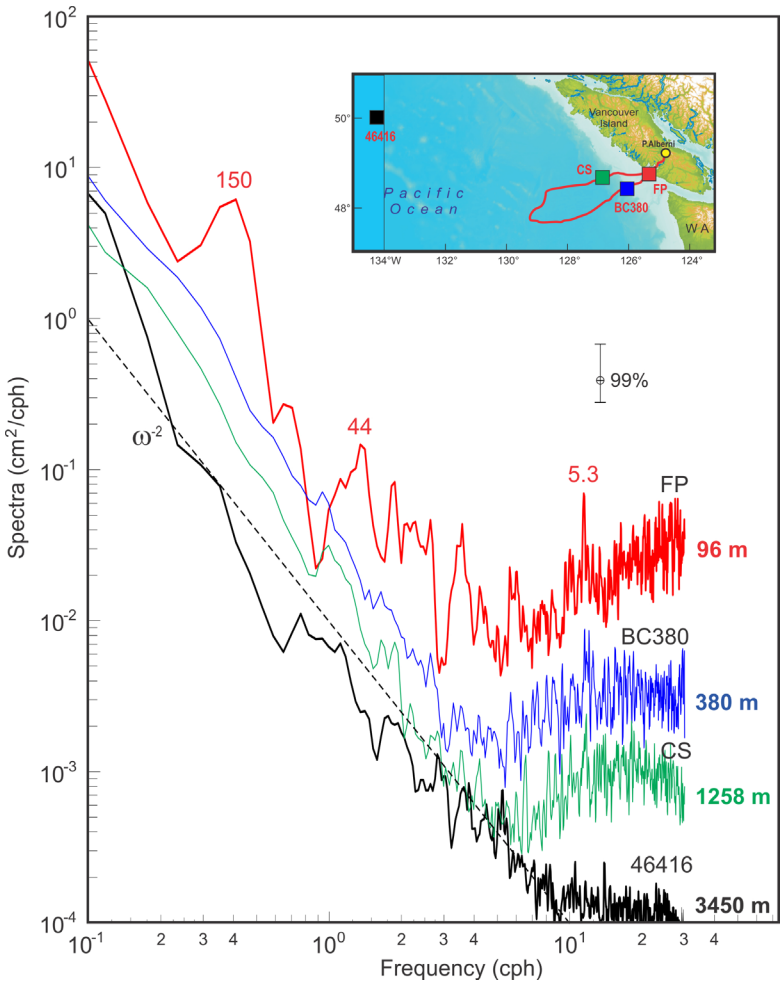

Figure 7. Open-ocean bottom pressure background spectra offshore from Vancouver Island for three ONC stations (FP = Folger Passage, BC380 = Barkley Canyon 380 m, and CS = Clayquot Slope) estimated for the period 10 – 20 October 2010 and DART 46416 for the period 9 – 22 August 2021. The locations of stations are shown in the inset. The dashed line indicates the ω^{-2} theoretical power law. The ONC spectra at frequencies > 6 cph (periods less than 10 min) are associated with storm-generated infragravity (IG) waves caused by the passage of typhoon Songda and two extratropical cyclones (described by *Rabinovich et al.* [2023a]). The depths of the corresponding instruments are denoted. The figure illustrates the modification of open-ocean sea level spectra with decreasing water depth and distance from the coast.

Figure 7 clearly illustrates that the background spectra become higher and more "jagged" with decreasing depth and proximity to the coast. The same effect for the Northwest Pacific region was described by *Rabinovich* [1997]. This is a universal property of longwave spectra: the closer to the coast, the smaller the depth, the more important is the impact of regional and local topography. The spectra shown in Figure 7 reflects the influence of slope and shelf on long waves arriving from the open ocean, emphasizing their transformation and amplification. This process plays a major role in formation of the destructive tsunamis affecting the coast [cf. *Hibiya and Kajiura*, 1981; *Monserrat et al.*, 2006]. Additionally, strong resonant amplification effects occur in bays, inlets and harbours [*Rabinovich*, 1993; 2009]. This is exactly what happened in Alberni Inlet during the 1964 Alaska tsunami (Figure 2), and what is regularly observed in Ciutadella Harbour, Menorca Island, Spain [*Monserrat et al.*, 1998], Nagasaki Bay, Japan [*Monserrat et al.*, 2006; *Rabinovich*, 2009] and in several other "hot spots" semi-enclosed basins, where devastating events regularly occur [cf. *Šepić and Rabinovich,* 2014; *Vilibić et al.*, 2016; *Rabinovich,* 2020].

The results of spectral analysis of ONC stations presented in Figure 7 allow us to estimate the amplification function $H(\omega)$ at each of the corresponding ONC sites relative to the open-ocean spectrum. However, the main purpose of our study is more specific: to examine resonant properties of coastal stations and to evaluate this function for all major tide gauge sites along the coast of British Columbia.

4. OBSERVATIONS AND *F-T* (WAVELET) ANALYSIS

We examined the resonant characteristics of sea level records from 16 CHS tide gauge sites shown in Figure 5. Distant trans-oceanic tsunamis, regional tsunamis and local meteotsunamis have been recorded many times at these sites [cf. *Rabinovich and Stephenson*, 2004; *Stephenson and Rabinovich*, 2009; *Rabinovich et al.*, 2006, 2013, 2019, 2023a]. These 16 stations we conditionally separated into two groups, South and North, with 8 stations in each group (Figure 5). For this analysis, we selected simultaneous one-month records from August 2023. This summer month is commonly calm; that is why it is good to study background oscillations not associated with significant storms, which are typical for winter months. The residual (de-tided) monthly records at all 16 records are shown in Figure 8. There were two cyclones passing over the region, one on 7-10 August and the other on 18 August, but they were not strong. However, the four southernmost stations, Point Atkinson, Patricia Bay, Victoria and Port Renfrew, on 29 August recorded prominent tsunami-like

waves, probably a meteotsunami (shaded area in Figure 8). This event requires an independent investigation. That is why, for the present spectral and wavelet analysis, the last three days of August were excluded.

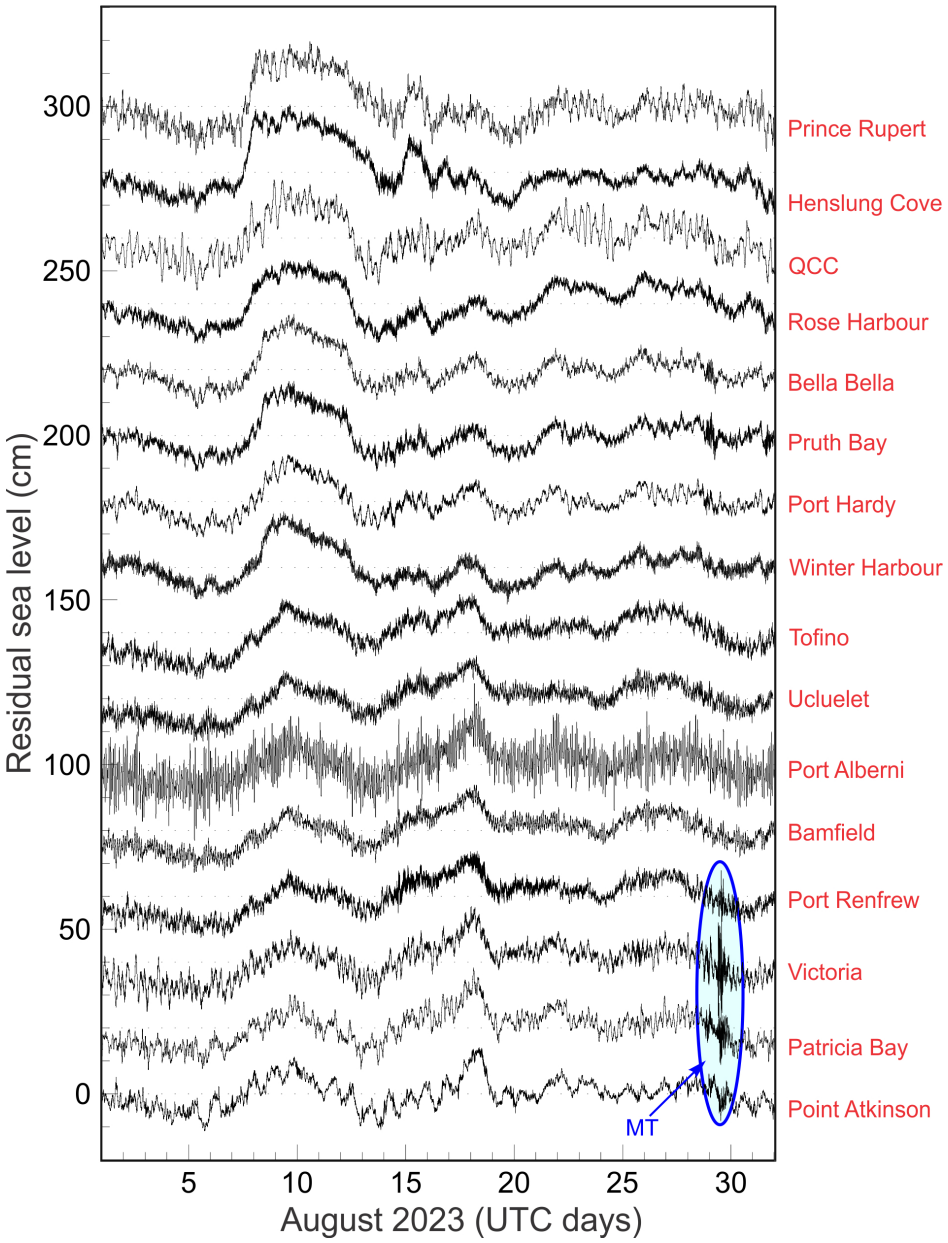

Figure 8. Residual (de-tided) tide gauge records for August 2023 for 16 CHS permanent stations on the coast of British Columbia (See Figure 5 for station locations). The records are shifted relative to each other by 20 cm. The shaded light blue area marks the meteotsunami that was observed at the four southernmost stations on 29 August.

To examine temporal variations of the sea level records in the frequency domain, we used a multiple-filter method, which is similar to wavelet analysis [*Thomson and Emery*, 2024). The method is based on narrow-band filters with a Gaussian window that isolates a specific centric frequency, $\omega_n = 2\pi f_n$, enabling us to determine changes in tsunami wave amplitudes as a function of frequency, *f*, and time, *t*, and to construct so called "*f-t* diagrams" that reveal possible dispersion effects and the nonstationary sea level variations [cf. *Rabinovich et al.*, 2006, 2013, 2019, 2023a; *Zaytsev et al.*, 2016, 2017, 2024]. In Figures 9 and 10, these diagrams are presented for the South and North tide gauge groups, respectively. The diagrams are constructed for the simultaneous time segments of 1 - 28 August 2023 for the frequency range 0.2 – 30 cph (periods from 5 hours to 2 minutes).

The *f-t* diagrams shown in Figures 9 and 10 confirm the significantly different character of sea level oscillations at different stations:

- At some stations, in particular, Prince Rupert, Port Alberni and Bella Bella, high-frequency (HF) oscillations are absent; at some others (e.g. Point Atkinson, Bamfield and Patricia Bay) they are present but much weaker than the low-frequency (LF) oscillations. It is obvious that waterways connecting these sites with the open ocean (Dixon Entrance, Alberni Inlet, Barkley Sound, Saanich Inlet, the Strait of Georgia, etc,) act as low-frequency filters that strongly suppress HF motions.

- Station Port Renfrew is strongly affected by motions with frequencies $>10^1$ cph (i.e., with periods <6 min) that appear to be related to IG-waves; it appears that this station is open to incoming ocean swell and storm waves, which normally are responsible for formation of these waves. The other stations are mostly sheltered from these waves and associated IG-motions.

- At several stations, the sea level oscillations occupy a relatively broad frequency band, from 0.4 to 6 cph (periods of 150-10 min) superimposed on narrow, well-defined and persistent frequency bands of significantly amplified energy that are likely associated with the eigen-frequencies of the corresponding sites.

- The *f-t* diagrams for certain stations provide clear evidence for a dominant frequency band, indicating a monochromatic nature of the oscillations. For example, we find dominant bands around ~0.6 cph (period of ~100 min) at Port Alberni, 0.4 cph (150 min) at Bamfield (Figure 9), 0.5 cph (120 min) at Prince Rupert and 2.5 cph (24 min) at Pruth Bay (Figure 10). At some other stations (in particular, Ucluelet, Victoria, Port Renfrew, Rose Harbour, Bella Bella, Henslung

Cove and Winter Harbour), there are two or even three enhanced frequency bands. We conclude that all of these stations have marked resonant properties. In contrast, such stations as Point Atkinson and Port Hardy do not reveal evident resonant features.

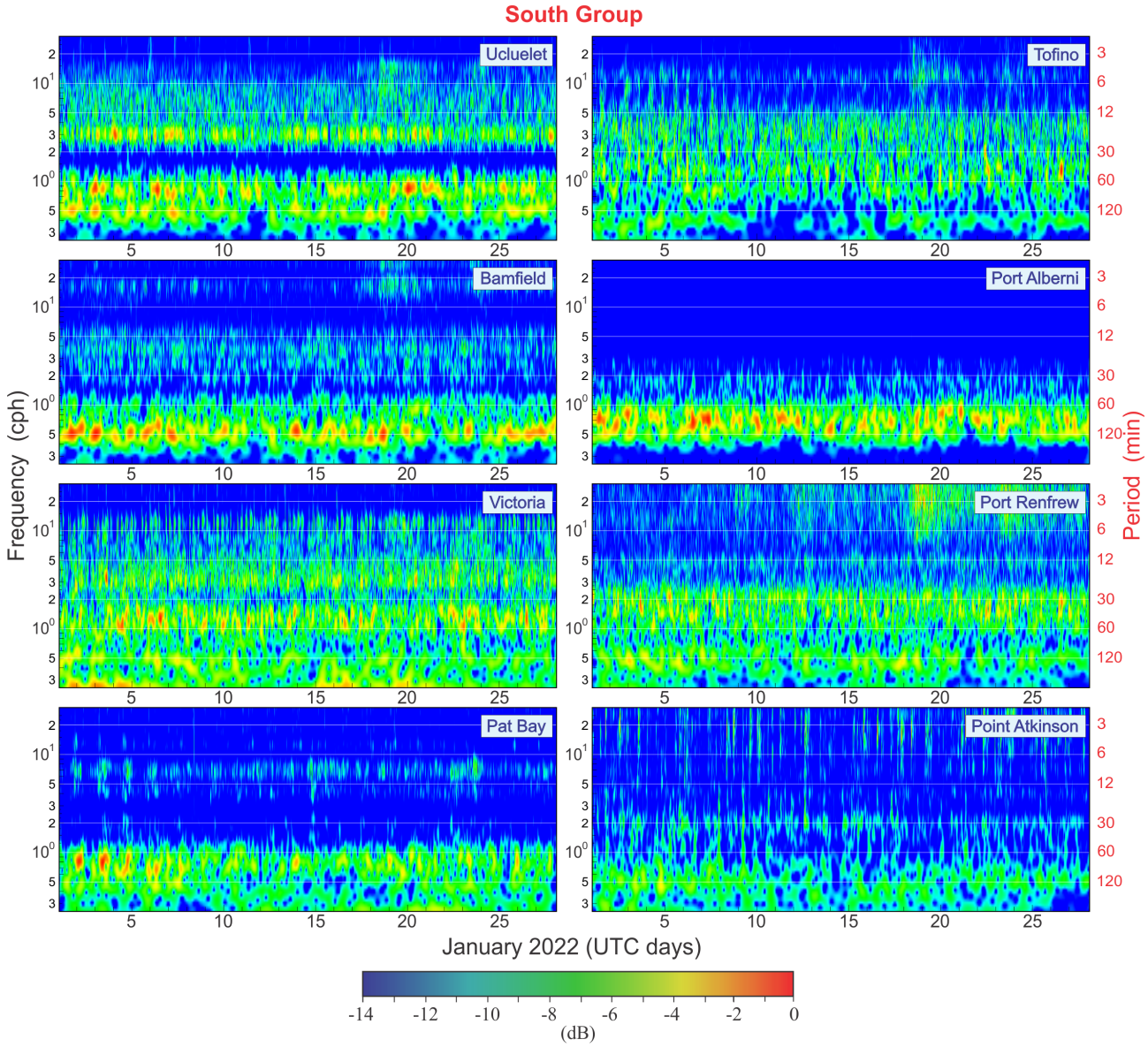

Figure 9. Frequency–time plots (*f*–*t* diagrams) for eight "South group" de-tided background sea level records for the period of 1 - 28 August 2023. Station locations are shown in Figure 5.

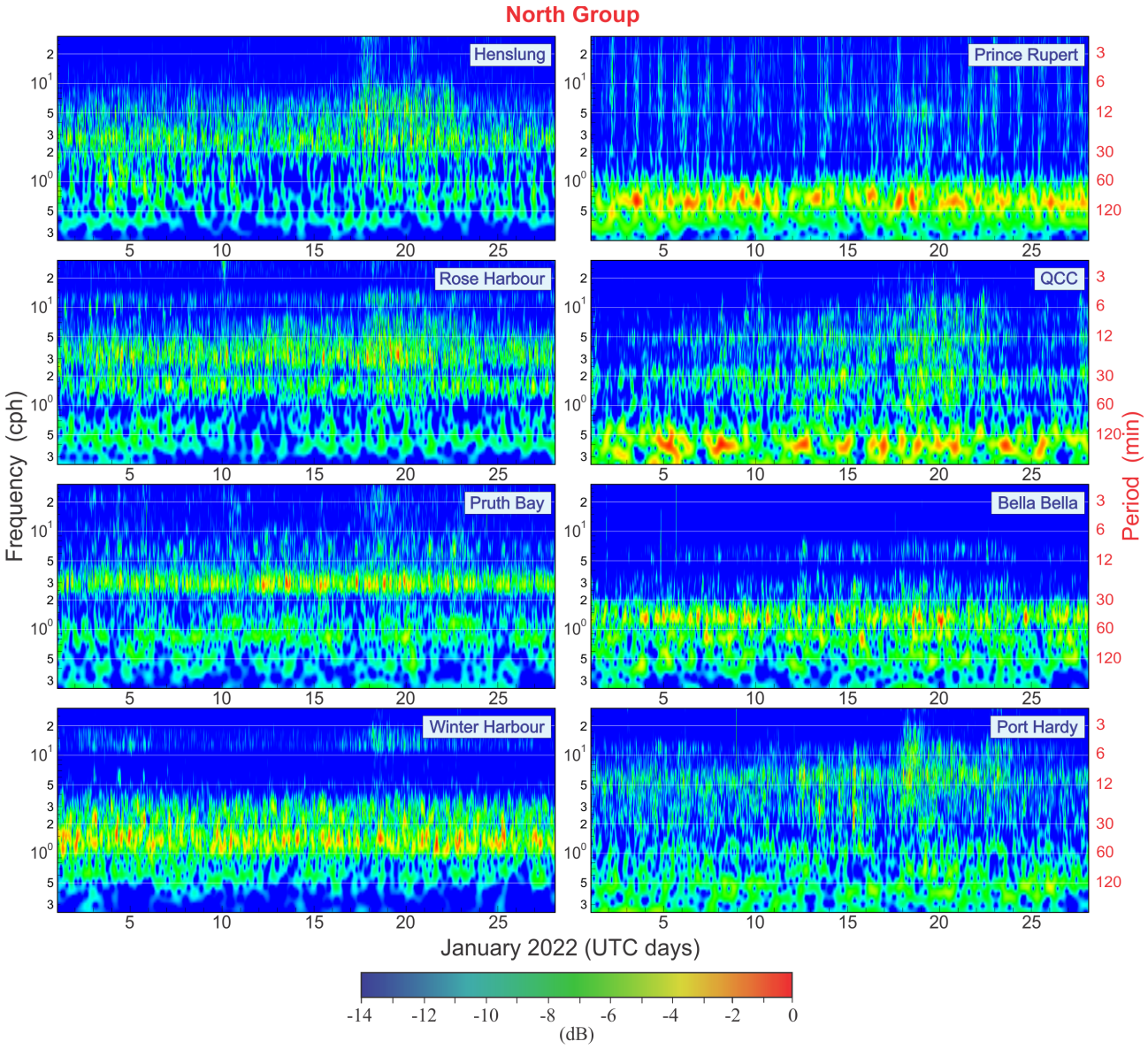

Figure 10. The same as in Figure 9 but for eight "North group" records. Station locations are shown in Figure 5.

5. ESTIMATION OF RESONANT CHARACTERISTICS FOR MAJOR COASTAL CHS SITES

It is possible to estimate the integral resonant properties of the individual sites much more precisely based on results of spectral analysis. For this purpose, we used the same 16 monthly sea-level de-tided records that we used for *f-t* analysis (Figures 8-10). To examine the spectral properties of these records, we employed the same approach used to examine many previous tsunamis [cf. *Rabinovich et al.,* 2013, 2017; *Zaytsev et al.*, 2016, 2017l 2024]. To improve the spectral estimates, a

Kaiser-Bessel (KB) spectral window with half-window overlaps was applied prior to the Fourier transform. The length of the series was 38880 min (27 days), the lengths of the spectral window was chosen to be N = 1024 min, yielding ν = 148 degrees of freedom; the spectral resolution was Δf = 0.0586 cph.

The derived spectra of the background sea level oscillations are shown in Figures 11 and 12. In general, the spectra are "*red*", with spectral energy decreasing with increasing frequency as ω^{-2}. This is typical for long wave sea level spectra not only for open-ocean (Figure 6 and 7) but also for coastal spectra [cf. *Rabinovich et al.*, 2013]. At the same time, there is a pronounced difference between the spectra for coastal (Figures 11 and 12) and deep-ocean (Figure 6) records. The open ocean background spectra are relatively smooth and monotonic; there are no prominent peaks in these spectra. The coastal spectra are more jagged, strongly variable from one station to another, and characterized by marked spectral peaks. These spectral peaks, which are different for each station, indicate the strong influence of topographic effects on coastal sea level oscillations. Because the periodicity of recorded tsunami waves is mainly related to the resonant properties of the local/regional topography rather than to frequency characteristics of the incoming waves, the spectra of tsunamis from different earthquakes are usually similar at the same location [cf. *Honda et al.*, 1908; *Miller*, 1972; *Rabinovich*, 1997]. In particular, the 2001 Peruvian, 2001 Queen Charlotte Islands, 2004 Sumatra and 2010 Chile tsunamis revealed quite similar spectral peaks [cf. *Rabinovich and Stephenson,* 2004; *Rabinovich et al.,* 2013].

Based on the results of our spectral analysis (Figures 11 and 12) and expressions (1) - (2) from Section 2, we estimated the amplification functions, $H_j(\omega)$, for all 16 examined sites. The A value was taken from the open-ocean spectra analysis (Figure 6): $A = 6.3\times10^{-3}$ cm^2·cph. The corresponding results are presented in Figures 13 and 14.

The computed functions $H_j(\omega)$ are significantly different, reflecting the individual resonant properties of each site. The most important conclusions, which can be made based analysis of these functions, are the following:

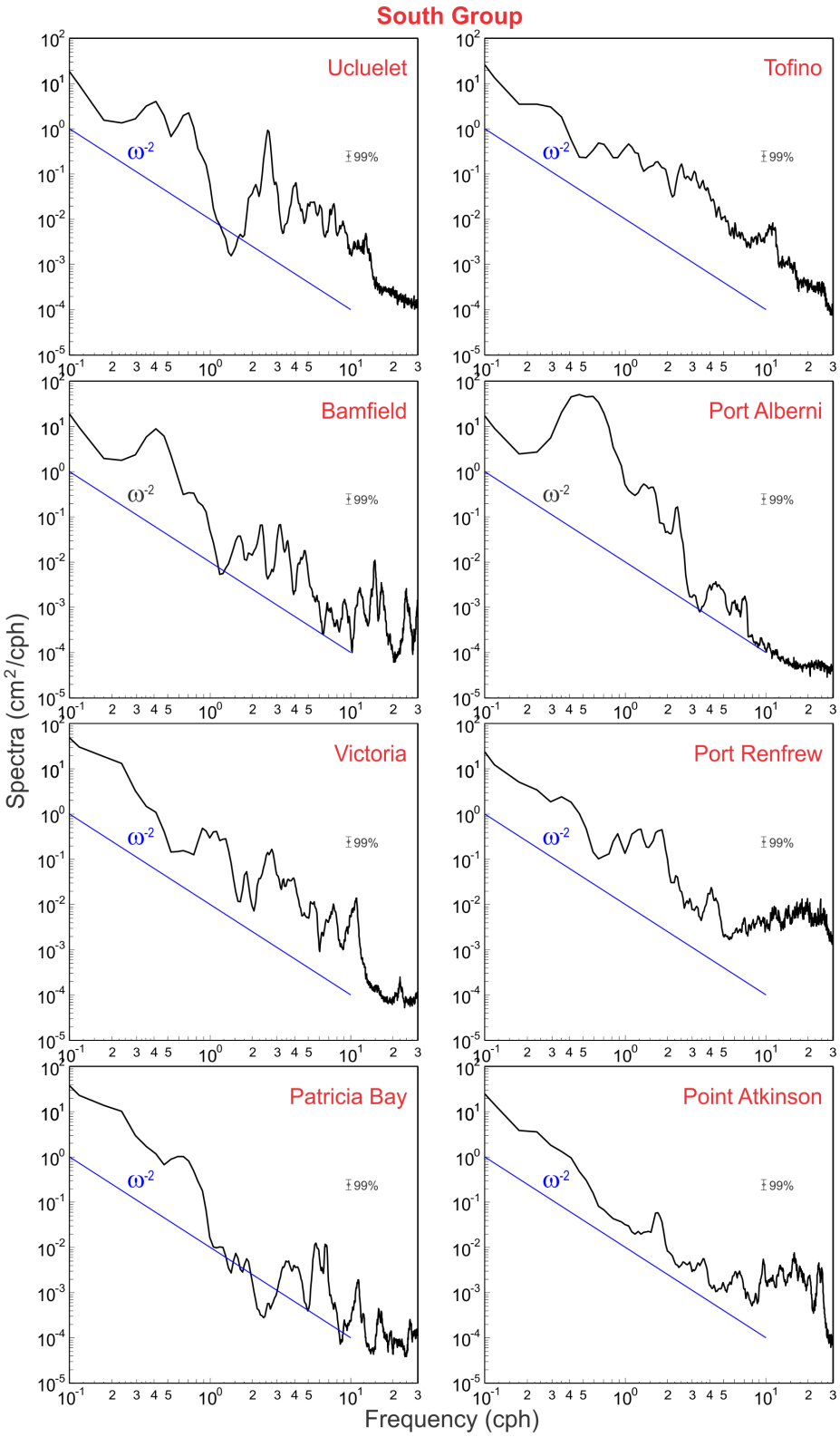

Figure 11. Spectra of background de-tided sea level oscillations at eight stations of the South group for the period 1–28 August 2023 (the period before the meteotsunami of 29 August 2023). The blue line indicates the ω^{-2} theoretical power law.

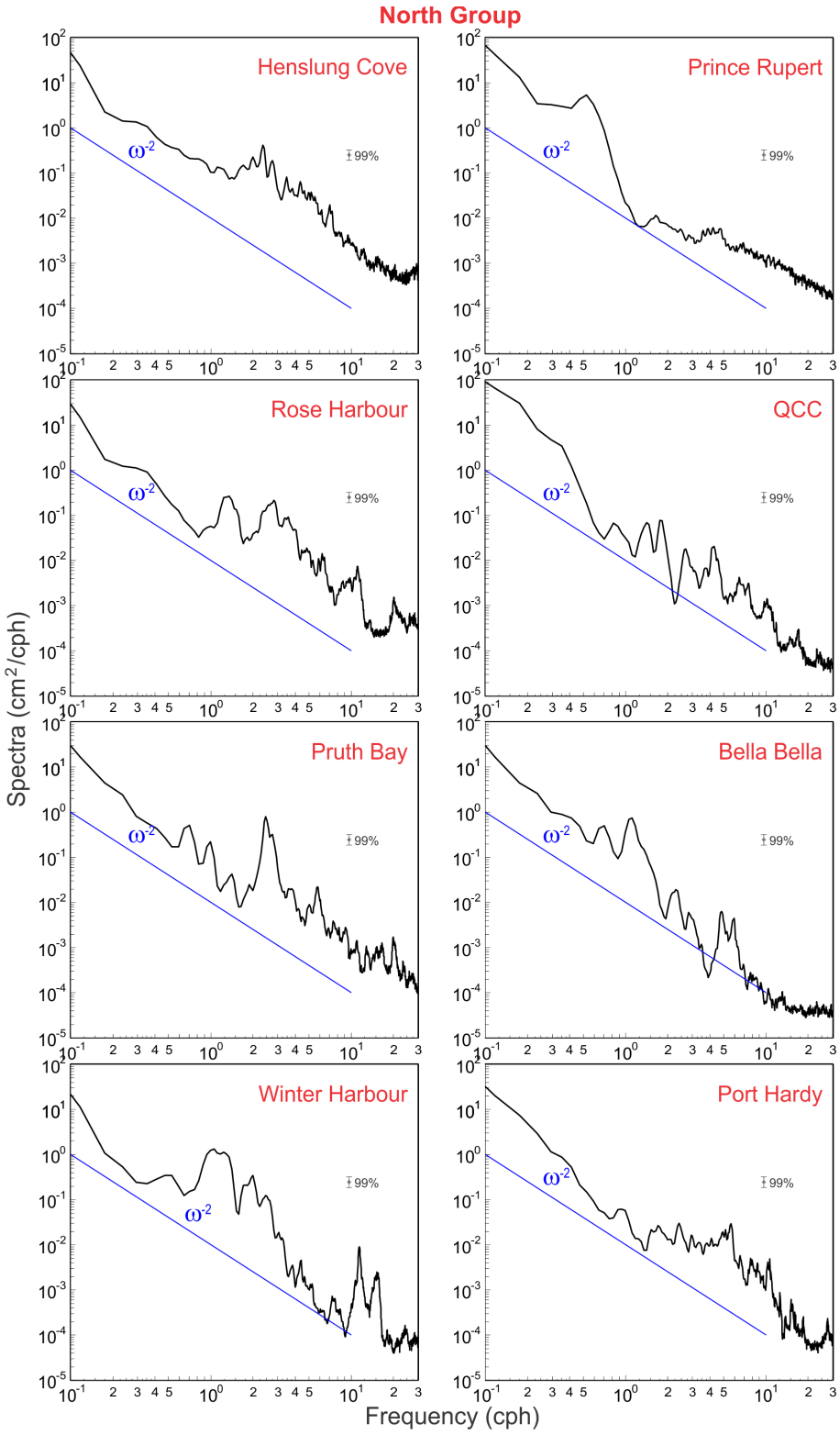

Figure 12. The same as in Figure 11 but for the eight “North group” stations.

- The maximum value $H_j(\omega)$ = **23.2** is observed at Port Alberni. The corresponding resonant period T_r = 102.4±5.2 min is in good agreement to what is shown in Figures 2, 3 and 4. According to *Rabinovich et al.* [2019], the 1964 Alaska tsunami waves arriving at the coast of British Columbia were *low-frequency* waves with dominant frequencies of 0.4–0.8 cph (periods of 2.5–1.2 h). Once again, this supports the earlier made assumption [cf. *Henry and Murty*, 1972. 1995; *Fine et al.*, 2009] that the 1964 event in Port Alberni was greatly amplified by topographically supported resonance within the waterway. These results further demonstrate that the resonant amplification of incoming waves at Port Alberni is stronger than at any other gauged site along the coast of British Columbia.

- Ucluelet (Figure 13) is another site a with very high value $H_j(\omega)$ = **14.5** at period T_r = 23 min. Specifically, destructive effects occurred at this site during the 2022 Tonga tsunami. The waves caused moderate damage to coastal infrastructure and severely damaged the community water line of the Ucluelet First Nations [*Rabinovich et al.*, 2023b]. It appears that all this was caused by the high *Q*-factor of the inlet and the strong amplification of arriving waves.

- One more site with $H_j(\omega)$ > 10.0 (i.e., one of the "hot spots") is Pruth Bay located in a fjord on the mainland coast. Here, $H_j(\omega)$ = **12.7** with T_r = 24.4 min (Figure 14).

- At several other stations – Henslung Cove, Rose Harbour, Port Renfrew, Bamfield, Victoria, Winter Harbour - $H_j(\omega)$ has sufficiently high values of 6.5 – 9.0 (Figures 13 and 14) indicating that all these sites are under considerable risk from tsunami waves.

- Specific attention should be paid to Prince Rupert. The amplification factor at this station, $H_j(\omega)$ = **7.1**, has a resonant period, T_r = 114 min (Figure 14). This is the only peak period, as high frequency oscillations at this station are strongly suppressed (see also Figure 10). Therefore, great earthquakes (with large source regions and associated long-period generated tsunami waves) can produce marked tsunamis at this site. The 1964 Great Alaska tsunami caused severe damage at Prince Rupert (although not as large as at Port Alberni), with a maximum trough-to-crest wave height of ~2.7 m [*Rabinovich et al.*, 2018, 2019].

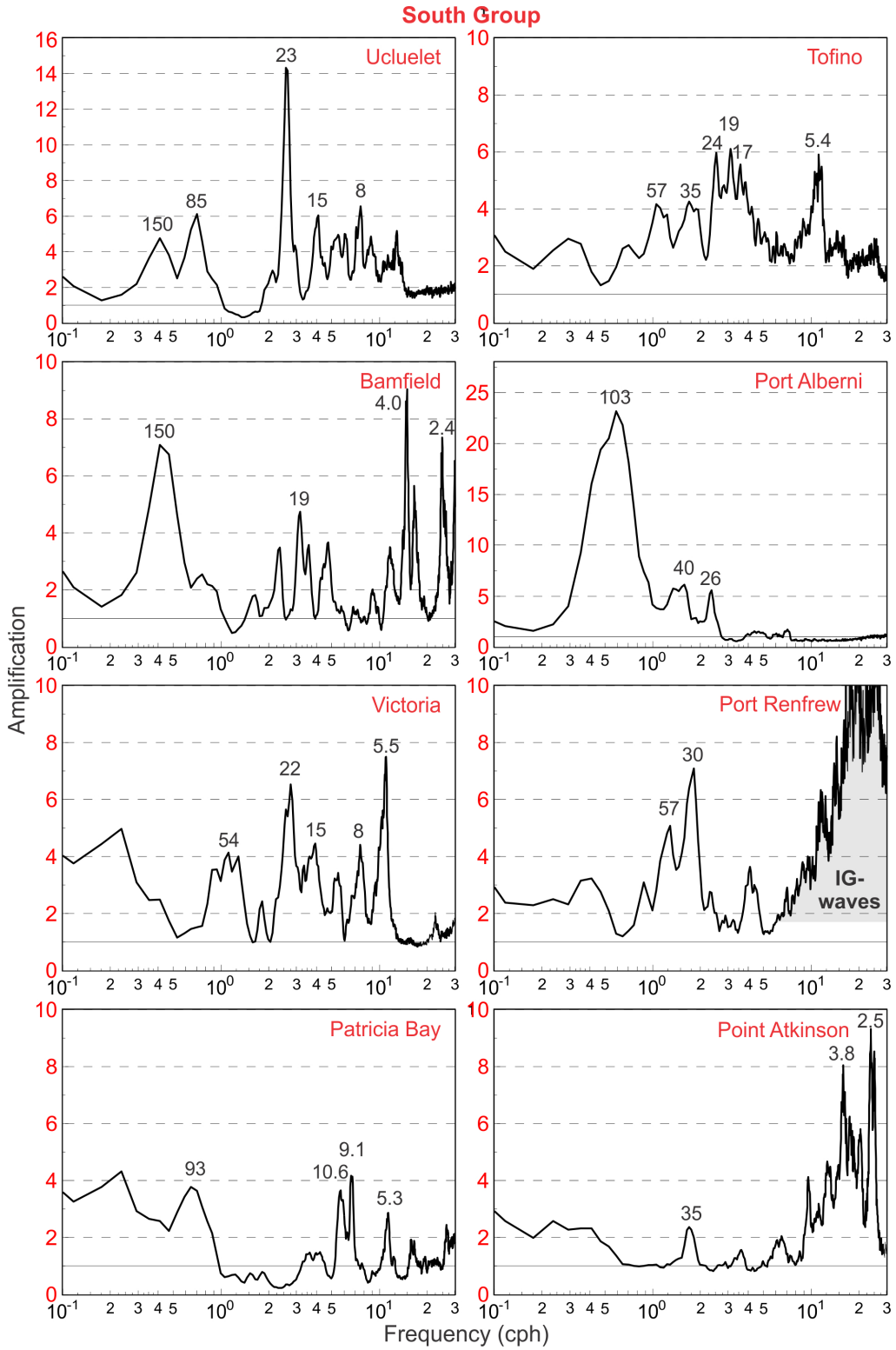

Figure 13. Amplification functions for eight stations of the South group estimated from the spectra shown in Figure 11. The numbers denote the main resonant periods (in min).

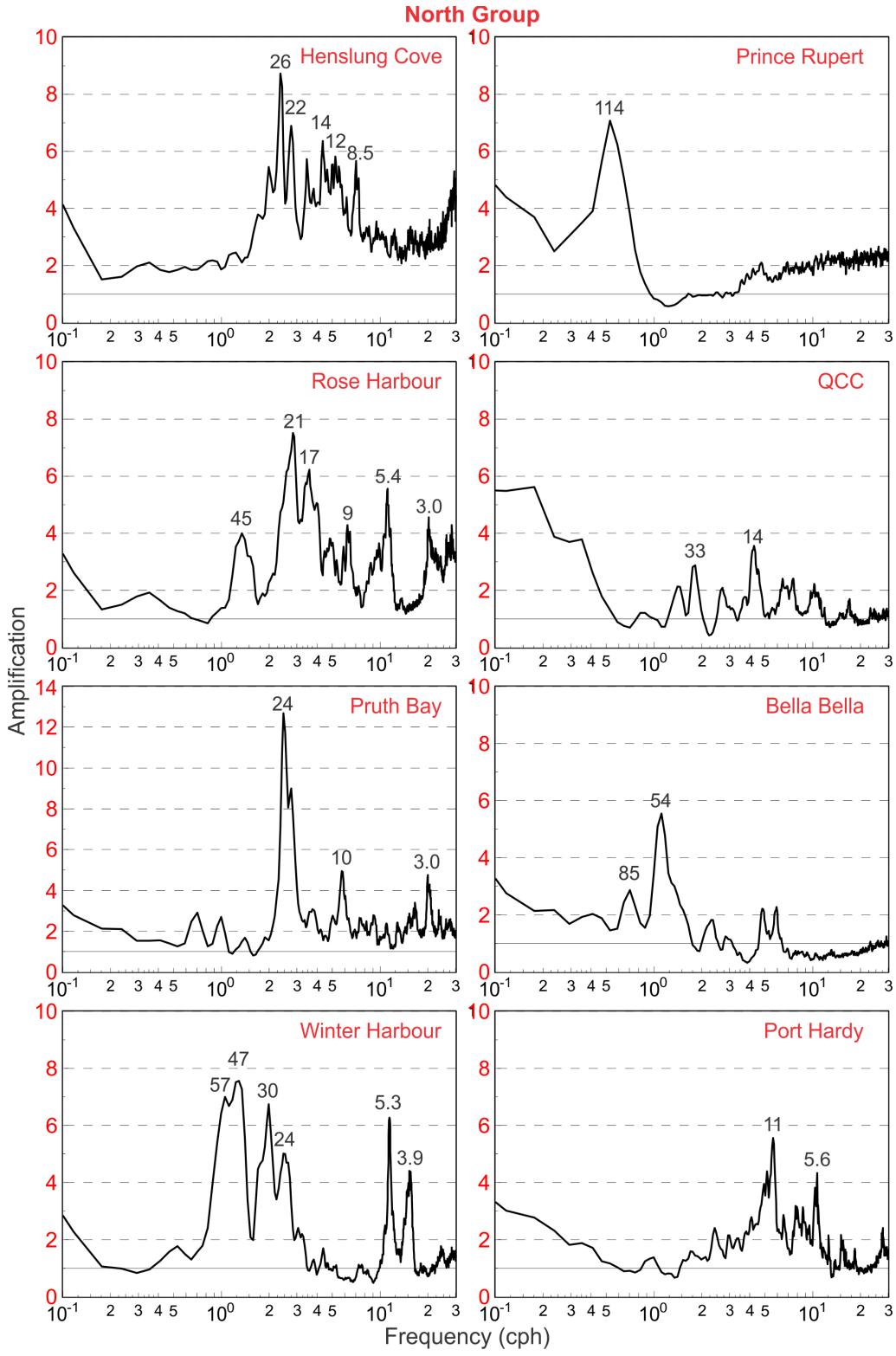

Figure 14. The same as in Figure 12 but for the eight “North group” stations.

- Another station of interest is Tofino. This station has one of the longest continuous sea level observation series in Canada (approximately 115 years) and has recorded more tsunamis than any other Canadian station [cf. *Wigen*. 1983; *Rabinovich et al.*, 2018, 2019]. From this point of view, this station may be considered as a "beacon station" that plays a key role in the Canadian Tsunami Warning Service. The amplification function at this site does not have one or two prominent peaks, but instead has a number of comparable peaks with $H_j(\omega)$ = **4.0 – 6.0** and resonant periods, T_r, from 5.4 to 57 min (Figure 13). This appears to be the reason why this station responses to a wide variety of tsunamis and even to meteotsunamis [cf. *Rabinovich et al.*, 2023].

- There are resonant peaks also at some other stations (e.g., Patricia Bay, Port Hardy, Bella Bella and QCC), but mostly they are smaller than at the sites listed above. Tsunami waves are regularly recorded at these stations and have specifically the same periods as those in the corresponding amplifications $H_j(\omega)$, but they are not destructive.

6. CONCLUSIONS

Long waves arriving from the open ocean can be strongly transformed and amplified by regional and local topography and bathymetry. At specific sites, "*hot-spots*", this amplification can be quite strong, and lead to destructive waves. The character of extreme sea level oscillations is determined by the specific geometry and physical features of the corresponding water basins, in particular, by the quality (Q) factors of these basins. Each closed or semi-closed basin has a set of natural (eigen) modes that are generated by external forcing and incoming open-ocean waves. Therefore, periods of observed tsunami waves are the same as those of regular background long waves recorded at the same site.

The coastline of British Columbia is complicated and has a diversity of topographic features, including islands, straits, bays, fjords and other waterways. These features strongly affect tsunami waves. While some of these features, such as the San Juan and Gulf islands, shelter parts of the Salish Sea from destructive tsunami waves, others can resonantly amplify these waves. Thus, on 28 March 1964, Port Alberni located at the head of long and narrow Alberni Inlet was severely impacted by the 1964 Alaska tsunami waves greatly enhanced within the inlet. Based on numerical modelling results of *Fine et al.* [2009], we examined resonant sea level oscillations within the system Barkley Sound–Alberni Inlet and confirmed the crucial influence of local topography on the character and

amplification of the open-ocean tsunami waves and the importance of the corresponding estimates along the coast of British Columbia.

Our analysis is based on DART and ONC open-ocean sea level observations offshore of southwestern Vancouver Island and on month-long coastal tide gauge observations at 16 major CHS sites for the common period of August 2023. The open-ocean background spectra in the tsunami frequency band of 0.3 – 8 cph (periods of 3.3 hr – 7.5 min) were smooth, monotonic, highly consistent and near exactly described by a ω^{-2} power law. Sea level oscillations $\zeta(t)$ recorded at time t by a tide gauge near the coast can be described as a convolution of the source $Z(t)$ and the topographic response function $w(t)$. In the spectral domain, this can be expressed in the form $S(\omega) = W(\omega)E(\omega)$, where ω is the angular frequency, $S(\omega)$ is the spectrum of the sea level record, $W(\omega) = H^2(\omega)$ is the admittance function, and $H(\omega)$ is the amplification function, describing the linear topographic transformation of long waves approaching the coast. The source function is given by the open spectrum as $E(\omega) = S_0(\omega) = A\omega^{-2}$, where A is estimated to be $A = 6.3\times10^{-3}$ cm^2·cph.

We evaluated the amplification function, $H_j(\omega)$, for all 16 selected CHS tide gauge sites. The maximum value $H_j(\omega)$ = **23.2** and resonant period T_r = 102.4±5.2 h was found to be at Port Alberni. This explains why this location was so strongly impacted by the 1964 tsunami. Significant values, $H_j(\omega)$ > 10.0, were also found at two other stations: Ucluelet ($H_j(\omega)$ = **14.5**, T_r = 23 min) and Pruth Bay ($H_j(\omega)$ = **12.7**, T_r = 24.4 min). All three sites may be characterized as "hot spots", i.e., as sites with anomalously strong responses to the external forcing (incoming open-ocean waves).

At several other stations, including Henslung Cove, Rose Harbour, Port Renfrew, Bamfield, Victoria and Winter Harbour, the maximum of amplification function, $H_j(\omega)$, was also high, values of 6.5 – 9.0, indicating that these sites are under considerable risk of tsunami waves.

Two more stations require specific attention. The amplification factor at Prince Rupert, $H_j(\omega)$ = **7.1**, the resonant period, T_r = 114 min. This low-frequency is the only peak period, while high-frequency oscillations at this station are strongly suppressed. Therefore, only great earthquakes with large source regions (like the 1964 Alaska event) can produce dangerous tsunami at this site; the 1964 Great Alaska tsunami caused severe damage at Prince Rupert. Another important station is Tofino, which has recorded more tsunamis than any other Canadian station and is can be designated as a "beacon station" for the Canadian Tsunami Warning Service. The amplification function at this site

has a number of comparable peaks with $H_j(\omega)$ = **4.0 – 6.0** and resonant periods, T_r, from 5.4 to 57 min. This appears to be the reason why this station responses to a broad variety of incoming tsunamis, including meteotsunamis.

There are resonant peaks also at some other stations (e.g., Patricia Bay, Port Hardy, Bella Bella and QCC), but mostly they are of smaller magnitude. Tsunami waves are regularly recorded at these stations and have specifically the same periods as those of $H_j(\omega)$ at these sites, but they are not destructive.

REFERENCES

Clague, J.J., Munro, A., and Murty, T.S. (2003), Tsunami hazard and risk in Canada, *Natural Hazards 28* (2-3), 407-434.

Djumagaliev, V.A., Rabinovich, A.B., and Fine, I.V. (1994), Theoretical and experimental estimation of transfer peculiarities of the Malokurilsk Bay coast, the Island of Shikotan, *Izvestiya, Atmospheric and Oceanic Physics*, 30(5), 680-686.

Fine, I.V., Cherniawsky, J.Y., Rabinovich, A.B., and Stephenson, F.E. (2009), Numerical modeling and observations of tsunami waves in Alberni Inlet and Barkley Sound, British Columbia, *Pure and Applied Geophysics*, *165*(11/12), 2019-2044.

Fine, I.V., Cherniawsky, J.Y., Thomson, R.E., Rabinovich, A.B., Krassovski, M.V. (2015), Observations and numerical modeling of the 2012 Haida Gwaii tsunami off the coast of British Columbia, *Pure and Applied Geophysics*, *172*(3-4), 699-718; doi: 10.1007/s00024-014-1012-7.

Henry, R.F., and Murty, T.S. (1972), Resonance periods of multi-branched inlets with tsunami amplification. Dep. Environ. Mar. Sci. Div., MS Rep. 28, 47-79.

Henry, R.F., and Murty, T.S. (1995), Tsunami amplification due to resonance in Alberni Inlet: Normal modes. In *Tsunami: Progress in Prediction, Disaster Prevention and Warning* (eds. Y. Tsushiya and N. Shuto), pp. 117-128, (Kluwer, Dordrecht).

Hibiya, T., & Kajiura, K. (1982). Origin of 'Abiki' phenomenon (kind of seiches) in Nagasaki Bay. *Journal of Oceanographical Society of Japan*, *38*, 172-182.

Honda, K., Terada, T., Yoshida, Y., and Isitani, D. (1908), An investigation on the secondary undulations of oceanic tides, *Journal of the College Science*, Imperial University of Tokyo, 108 pp.

Imamura, F. (1996), Review of tsunami simulation with a finite difference method. In *Long Wave Runup Models* (eds. H. Yeh, P. Liu, and C. Synolakis), pp. 25-42 (World Scientific Publishing, Hackensack, N.J.

Kovalev, P.D., Rabinovich, A.B., and Shevchenko, G.V. (1991), Investigation of long waves in the tsunami frequency band on the southwestern shelf of Kamchatka, *Natural Hazards*, *4*(2/3), 141-159.

Kulikov, E.A., Rabinovich, A.B., Spirin, A.I., Poole, S.L., and Soloviev, S.L. (1983), Measurement of tsunamis in the open ocean, *Marine Geodesy*, *6*(3-4), 311-329.

Lee, J.J. (1971), Wave induced oscillations in harbors of arbitrary geometry, *Journal of Fluid Mechanics*, *45*, 375–394.

Loomis, H.G. (1966), Spectral analysis of tsunami records from the stations in the Hawaiian Islands, *Bulletin of the Seismological Society of America, 56*(3), 697-713.

Mei, C.C. (1992), *The Applied Dynamics of Ocean Surface Waves*, World Scientific, London, 740 pp.

Miller, G.R. (1972), Relative spectra of tsunamis. Hawaii Institute of. Geophysics, HIG-72-8, 7 pp.

Mofjeld, H. O., González, F. I., and Newman, J. C. (1999), Tsunami prediction in U.S. coastal regions, In: C. N. K. Mooers (ed.), *Coastal Ocean Prediction, Coastal and Estuarine Studies*, *56*, AGU, Washington, pp. 353–375.

Mofjeld, H. O., González, F. I., Bernard, E. N., and Newman, J. C. (2000), Forecasting the heights of later waves in Pacific-wide tsunamis, *Natural Hazards*, *22*, 71–89.

Monserrat, S., Rabinovich, A.B., and Casas, B. (1998), On the reconstruction of the transfer function for atmospherically generated seiches, *Geophysical Research Letters, 25*, 2197–2200 (1998).

Monserrat, S., Vilibić, I., & Rabinovich, A.B. (2006), Meteotsunamis: Atmospherically induced destructive ocean waves in the tsunami frequency band. *Natural Hazards and Earth System Sciences*, *6*, 1035-1051.

Mungov, G., Eblé, M., and Bouchard, R. (2013), DART tsunameter retrospective and real-time data: A reflection on 10 years of processing in support of tsunami research and operations, *Pure and Applied Geophysics, 170*, 1369-1384. https://doi.org/10.1007/s00024-012-0477-5

Murty, T. S. (1977), *Seismic Sea Waves – Tsunamis*, Bull. Fish. Res. Board Canada 198, 337 pp.

Murty, T. S. (1992), Tsunami threat to the British Columbia coast, In *Geotechnique and Natural Hazards*, BiTech. Publ., Vancouver, BC, pp. 81–89.

Murty, T. S. and Boilard, L. (1970), The tsunami in Alberni Inlet caused by the Alaska earthquake of March, 1964. In *Tsunami in the Pacific Ocean* (ed. W.M. Adams) pp. 165-187 (East West Center Press, Honolulu, HI).

Pugh, D. & Woodworth, P. (2014), *Sea-Level Science: Understanding Tides, Surges, Tsunamis and Mean Sea-Level Changes*. Cambridge Uni. Press, 395 pp. https://doi.org/10.1017/CBO9781139235778

Rabinovich, A.B. (1997), Spectral analysis of tsunami waves: Separation of source and topography effects, *Journal of Geophysical Research*, *102*(C6), 12,663-12,676.

Rabinovich, A.B. (2009), Seiches and harbor oscillations. In *Handbook of Coastal and Ocean Engineering* (Ed. Kim, Y. C.), 193-236 (World Scientific Publ.).

Rabinovich, A.B. (2020), Twenty-seven years of progress in the science of meteorological tsunamis following the 1992 Daytona Beach event, *Pure and Applied Geophysics,* 177(3), 1193-1230; doi: 10.1007/s00024-019-02349-3.

Rabinovich, A.B., Monserrat, S. and Fine, I.V. (1999), Numerical modeling of extreme seiche oscillations in the region of the Balearic Islands, *Oceanology*, *39*(1), 16-24.

Rabinovich, A.B., and Stephenson, F.E. (2004), Longwave measurements for the coast of British Columbia and improvements to the tsunami warning capability, *Natural Hazards*, *32*(3), 313-343.

Rabinovich, A.B., Thomson, R.E., and Stephenson, F.E. (2006), The Sumatra tsunami of 26 December 2004 as observed in the North Pacific and North Atlantic oceans, *Surveys in Geophysics*, *27*, 647-677.

Rabinovich, A.B., Thomson, R.E. and Fine, I.V. (2013), The 2010 Chilean tsunami off the west coast of Canada and the northwest coast of the United States, *Pure and Applied Geophysics*, *170*, 1529-1565, doi 10.1007/s00024-012-0541-1.

Rabinovich, A.B., Titov, V.V., Moore, C.W., and Eblé, M.C. (2017), The 2004 Sumatra tsunami in the southeastern Pacific Ocean: New global insight from observations and modeling, *Journal of Geophysical Research - Oceans*, *122*(10), 7992-8019; doi: 10.1002/2017JC013078.

Rabinovich, A.B., Thomson, R.E., Lupton, L.M., and Mundschutz, S. (2018). *Historical Tsunamis at the Seal Cove and Victoria Canadian Coast Guard Stations, British Columbia*. Can. Tech. Rep. Hydrogr. Ocean Sci. 325: ix + 44p.

Rabinovich, A.B., Thomson, R.E., Krassovski, M.V., Stephenson, F.E., and Sinnott, D.C. (2019), Five great tsunamis of the 20th century as recorded on the coast of British Columbia, *Pure and Applied Geophysics*, *176*(7), 2887-2924; doi: 10.1007/s00024-019-02133-3.

Rabinovich, A.B., Šepić, J., and Thomson, R.E (2023a), Strength in numbers: The tail end of typhoon Songda combines with local cyclones to generate extreme sea level oscillations on the British Columbia and Washington Coasts during Mid-October 2016, *Journal of Physical Oceanography*, *53*(1), 131-155; doi:10.1175/JPO-D-22-0096.1.

Rabinovich, A., Sinnott, D., and Thomson, R. (2023b). Tsunami Risk at Ucluelet Harbour, British Columbia. Can. Tech. Rep. Hydrogr. Ocean Sci. 373: v + 25 p.

Raichlen, F., Lepelletier, T. G., and Tam, C. K. (1983), The excitation of harbors by tsunamis, In K. Iida and T. Iwasaki (eds), *Tsunamis – Their Science and Engineering*, Terra Sci., Tokyo, pp. 359–385.

Šepić, J., & Rabinovich, A.B. (2014), Meteotsunami in the Great Lakes and on the Atlantic coast of the United States generated by the ‘‘derecho’’ of June 29–30, 2012, *Natural Hazards*, 74, 75-107; doi: 10.1007/s11069-014-1310-5.

Stephenson, F.E., and Rabinovich, A.B. (2009), Tsunamis on the Pacific coast of Canada recorded in 1994-2007, *Pure and Applied Geophysics*, *166*(1/2), 177-210.

Thomson, R.E. (1981) (Reprinted 1983, 1984, 1991) *Oceanography of the British Columbia Coast.* Can. Special Pub. Fish. Aquat. Sci., 56. Ottawa, 291p.

Thomson, R., Fine, I., Rabinovich, A., Mihály, S., Davis, E., Heesemann, M., and Krassovski, M. (2011), Observation of the 2009 Samoa tsunami by the NEPTUNE-Canada cabled observatory: Test data for an operational regional tsunami forecast model, *Geophysical Research Letters*, *38*, L11701, doi:10.1029/2011GL046728.

Thomson R.E., and Emery, W.J. (2024*). Data Analysis Methods in Physical Oceanography*, Fourth Edition. Elsevier, New York, 874 p. https://doi.org/10.1016/B978-0-323-91723-0.00010-6.

Thomson, R., Rabinovich, A., Lupton, L., Mundschutz, S., and Hastings, N., 2023. *Effect of Global Sea Level Rise over the Near, Intermediate and Long-Term on Tsunami Waves at the Seal Cove Coast Guard Station in Northwestern British Columbia*. Can. Tech. Rep. Hydrogr. Ocean Sci. 361: v + 75 p.

Vilibić, I., Šepić, J., Rabinovich, A.B., and Monserrat, S. (2016). Modern approaches in meteotsunami research and early warning. *Frontiers in Marine Science*, 3 (57), 1-7; doi: 10.3389/fmars.2016.00057.

Wigen, S. O. and White, W. R. H. (1964), *Tsunami of March 27–29, 1964, West Coast of Canada*, Unpublished manuscript, 6 pp, (Department of Mines and Technical Surveys, Ottawa, 1964).

Wigen, S. O. (1983), Historical studies of tsunamis at Tofino, Canada, In: K. Iida and T. Kawasaki (eds), *Tsunamis – Their Science and Engineering*, Terra Sci. Publ. Comp., Tokyo, Japan, pp. 105–119

Zaytsev, O., Rabinovich, A.B., and Thomson, R.E. (2016), A comparative analysis of coastal and open-ocean records of the great Chilean tsunamis of 2010, 2014 and 2015 off the coast of Mexico. *Pure and Applied Geophysics*, *173*(12), 4139-4178; doi: 10.1007/s00024-016-1407-8.

Zaytsev, O., Rabinovich, A.B., and Thomson, R.E. (2017), The 2011 Tohoku tsunami on the coast of Mexico: A case study. *Pure and Applied Geophysics*, *174*(8), 2961-2986; doi: 10.1007/s00024-017-1593-z.

Zaytsev, O., Rabinovich, A.B., and Thomson, R.E. (2024). The 2022 Tonga tsunami on the Pacific and Atlantic coasts of the Americas. *Journal of Geophysical Research: Oceans*, *129*, e2024JC020926. https://doi.org/10.1029/2024JC020926.